JACS
JOURNAL OF THE AMERICAN CHEMICAL SOCIETY
Article
pubs.acs.org/JACS

Metal Nitrides Grown from Ca/Li Flux: $Ca_6Te_3N_2$ and New Nitridoferrate(I) $Ca_6(Li_xFe_{1-x})Te_2N_3$

Matthew J. Dickman and Susan E. Latturner*

Department of Chemistry, Florida State University, Tallahassee Florida 32308, United States

Supporting Information

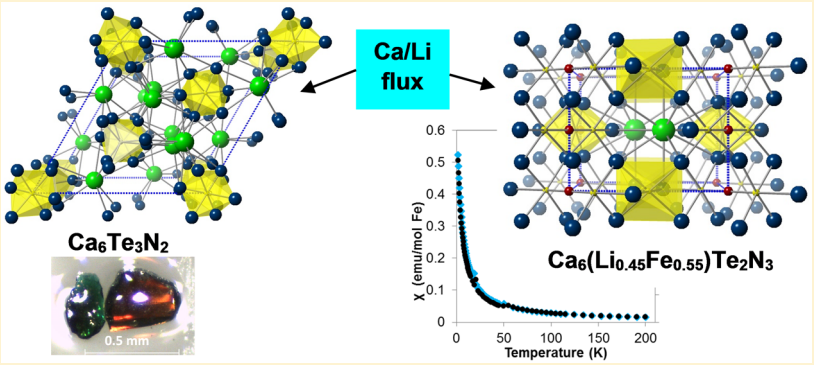

ABSTRACT: Two new tellurium-containing nitrides were grown from reactions in molten calcium and lithium. The compound $Ca_6Te_3N_2$ crystallizes in space group $R\bar{3}c$ (a = 12.000(3)Å, c = 13.147(4)Å; Z = 6); its structure is an anti-type of rinneite ($K_3NaFeCl_6$) and 2H perovskite related oxides such as $Sr_3Co_2O_6$. The compound $Ca_6(Li_xFe_{1-x})Te_2N_3$ where $x \approx 0.48$ forms in space group $P4_2/m$ (a = 8.718(3)Å, c = 6.719(2)Å; Z = 2) with a new stuffed anti-type variant of the Tl_3BiCl_6 structure. Band structure calculations and easily observable red/green dichroic behavior indicate that $Ca_6Te_3N_2$ is a highly anisotropic direct band gap semiconductor (E_g = 2.5 eV). $Ca_6(Li_xFe_{1-x})Te_2N_3$ features isolated linear N−Fe−N units with iron in the rare Fe^{1+} state. The magnetic behavior of the iron site was characterized by magnetic susceptibility measurements, which indicate a very high magnetic moment (5.16μ_B) likely due to a high degree of spin−orbit coupling. Inherent disorder at the Fe/Li mixed site frustrates long-range communication between magnetic centers.

INTRODUCTION

Binary nitride materials have been valued for their versatile physical properties since the early 20th century. Gallium nitride and its III−V solid solutions are semiconductors widely used in light-emitting diode and laser technology.[1−3] Transition metal binary nitrides such as NbN and TiN are well-known for their superconductivity, Fe_4N and $Fe_{16}N_2$ have useful magnetic properties, W_2N, Mo_2N, MoN_2, and Ta_3N_5 are potential catalysts, and MoN and Re_3N are known for their mechanical properties.[4−13] More recently ternary nitrides such as $AgTaN_2$, MAX nitride phases (such as V_2GaN and Ti_4AlN_3), $Li_2[(Li_{1-x}Fe_x)N]$ (x = 0.63), and others are gathering interest due to their unique physical properties.[14−17]

Unfortunately, complex metal nitrides are very difficult to synthesize. Elemental nitrogen has a sturdy triple bond and conversion of atomic nitrogen to N^{3-} has a high energy cost. Metal nitrides are thermodynamically unstable with respect to their corresponding oxides. These factors make the formation of nitrides a greater challenge than most materials such as the ubiquitous oxide families. Therefore, the ability to overcome these barriers presents a great opportunity to discover new compounds with unique properties.

Synthetic techniques that have been explored to solve this problem include conventional solid state reaction, ammonolysis, vapor deposition methods, solid−solid phase metathesis reaction, magnetron sputtering, and growth from metal or salt fluxes.[18−21] The metal flux method involves the use of an excess of a low melting metal as a solvent; this dissolves reactants and facilitates reactions by eliminating diffusion barriers. We are exploring flux mixtures of calcium and lithium. Calcium has a melting point above 800 °C, but when combined with lithium in a 1:1 mol ratio, a molten mixture forms at a significantly lowered temperature of about 300 °C. While electronegative main group elements are especially soluble in electropositive Ca/Li mixtures, light elements are also highly reactive in these melts. Previous reactions utilizing Ca/Li flux have produced compounds such as $Ca_{12}InC_{13-x}$, $Ca_{54}In_{13}B_{(4-x)}H_{(23+x)}$, $Ca_{11}E_3C_8$ (E = Sn, Pb), $LiCa_3As_2H$, $LiCa_7Ge_3H_3$, and Ca_2LiC_3H.[22−27] Based on the successful syntheses of complex metal carbides and hydrides from refractive light element sources, it was postulated that Ca/Li flux may also be useful for the synthesis of complex nitrides.

Received: June 11, 2016
Published: August 1, 2016

DOI: 10.1021/jacs.6b06024
J. Am. Chem. Soc. 2016, 138, 10636−10644

Table 1. Crystallographic Data Collection Parameters for the Title Phases

	$Ca_6Li_{0.48}Fe_{0.52}Te_2N_3$	$Ca_6Te_3N_2$
formula wt (g/mol)	571.1	651.3
cryst syst	tetragonal	rhombohedral
space group	$P4_2/m$ (#84)	$R\bar{3}c$ (#167)
a (Å)	8.718(3)	12.000(3)
c (Å)	6.719(2)	13.147(4)
Z	2	6
volume (Å^3)	510.7(4)	1639.5(10)
density, calcd (g/cm^3)	3.709	3.958
index ranges	$-11 \le h \le 11$, $-11 \le k \le 11$, $-8 \le l \le 5$	$-15 \le h \le 16$, $-16 \le k \le 15$, $-17 \le l \le 17$
reflns collected	3742	6417
unique data/params	691/38	456/20
μ (mm^{-1})	9.38	10.71
R_1/wR_2[a]	0.0194/0.0495	0.0111/0.0246
R_1/wR_2 (all data)	0.0196/0.0499	0.0120/0.0249
GOF	1.400	1.091

[a] $R_1 = \sum(|F_o| - |F_c|)/\sum|F_o|$; $wR_2 = [\sum[w(F_o^2 - F_c^2)^2]/\sum(w|F_o|^2)^2]^{1/2}$.

Two new complex metal nitrides, $Ca_6Te_3N_2$ and $Ca_6(Li_xFe_{1-x})Te_2N_3$ (with $x \approx 0.48$), were grown from reactions of tellurium and an ionic nitride source in Ca/Li flux. Both compounds exhibit charge-balancing with Te^{2-} anions and N^{3-} anions surrounded by Ca^{2+} cations. Additionally, $Ca_6(Li_xFe_{1-x})Te_2N_3$ contains a Li/Fe[1] mixed site linearly coordinated by two nitride anions. Iron as the Fe^+ species in iron-substituted Li_3N has been reported to exhibit a uniquely high magnetic moment; magnetic susceptibility measurements confirm that such behavior is also present in $Ca_6(Li_xFe_{1-x})Te_2N_3$.[28,29] $Ca_6Te_3N_2$ has a rhombohedral structure and exhibits strong red/green dichroism. Band structure calculations for $Ca_6Te_3N_2$ were carried out to investigate the potential cause of the dichroism and confirm the anisotropic nature of the band gap.

EXPERIMENTAL PROCEDURE

Synthesis. $Ca_6Te_3N_2$ was initially observed as a low yield byproduct of reactions of tellurium and carbon in Ca/Li flux. Calcium metal (99.5%, Alfa Aesar), chunks of lithium (99.8% Strem), tellurium powder (99.95%, CERAC), and acetylene carbon black powder (99.5% Alfa Aesar) were used as received. Reactants and flux metals were added to stainless steel crucibles (7.0 cm length/0.7 cm diameter) in a 7:7:1:2 mmol Ca/Li/Te/C ratio in an argon-filled glovebox. The crucibles were sealed by arc-welding under argon and were placed in silica tubes, which were flame-sealed under vacuum. The ampules were heated from room temperature to 1050 °C in 3 h and held there for 2 h. The reactions were cooled stepwise to 850 °C in 72 h and to 500 °C in 36 h, and then held at 500 °C for 24 h. The reactions were then removed from the furnace, inverted, and centrifuged for 2 min to separate the crystalline products from the Ca/Li melt. Crystal products adhere to the sides of the crucible. The steel crucibles were cut open in an argon-filled glovebox.

Initial crystallographic studies of the product indicated that light element sites were occupied by nitrogen instead of carbon. Since some of the reactions were carried out using calcium metal that was purified by heating to 700 °C under high vacuum to remove any hydride and nitride contaminants that could possibly mix onto light element sites, the likely nitride source was the lithium metal reactant (which has a thin nitride surface film). Subsequent reactions were prepared (similarly to those mentioned in the previous paragraph) using deliberately added Li_3N (99.5% CERAC) or Ca_3N_2 (99% CERAC) as a nitride source. The reaction Ca/Li/Te/Li_3N (in a 7:7:1:1 mmol ratio) produced a significantly higher yield of $Ca_6Te_3N_2$, but it also resulted in formation of the byproduct $Ca_6(Li_xFe_{1-x})Te_2N_3$, obtained in low yield. To ensure no carbon from the steel crucible mixed onto light element sites, Ca/Li/Te/Li_3N or Ca/Li/Te/Ca_3N_2 (both reactions in a 3.5:3.5:0.5:0.5 mmol ratio) were prepared in sealed niobium crucibles. Reproduction of the desired $Ca_6Te_3N_2$ was successful, which confirms the identity of the atom at the light element sites to be nitrogen (see crystal data, vide infra). It is noteworthy that the use of Li_3N produced $Ca_6Te_3N_2$ in low yield (with CaTe as the major phase), while the use of Ca_3N_2 as the nitride source produced $Ca_6Te_3N_2$ as the major product. Using niobium also excludes iron from the reaction mixture, so no $Ca_6(Li_xFe_{1-x})Te_2N_3$ formed in these reactions.

$Ca_6(Li_xFe_{1-x})Te_2N_3$ was formed from leaching of iron from the stainless steel crucible during the reaction. Leaching is exacerbated by adding carbon into the reaction. Ca/Li/Te/C/Li_3N reactions in a 7:6:1:2:1 mmol ratio produce almost pure $Ca_6(Li_xFe_{1-x})Te_2N_3$ with no $Ca_6Te_3N_2$; the only byproducts were slight amounts of carbon powder and CaTe (see powder X-ray diffraction data in Supporting Information, Figure S1). The EDS data indicated some nickel present in the material, likely mixing on the iron site. To determine whether the compound could be prepared without nickel or carbon incorporation, the reaction Ca/Li/Te/Li_3N/Fe foil in a 3.5:3.5:0.5:0.5:1 mmol ratio was prepared in a niobium crucible. $Ca_6(Li_xFe_{1-x})Te_2N_3$ was reproduced, albeit in low yield (several competing phases were present such as CaTe and $CaLi_2$). This shows the compound can be produced without any incorporation of nickel. This also confirms single crystal refinements suggesting light element sites are indeed occupied by nitrogen.

Elemental Analysis. Elemental analyses were carried out using a scanning electron microscope (SEM; FEI NOVA 400) with energy dispersive spectroscopy (EDS) capabilities. Samples of product crystals were affixed to an aluminum SEM stub using carbon tape and analyzed using a 30 kV accelerating voltage. The EDS detector is not sensitive to the presence of light elements such as lithium or nitrogen, so only the relative ratios of calcium, tellurium, iron, and nickel were observed. The presence of lithium and nitrogen within the crystal structure was inferred based on reactants present, bond lengths observed, and charge balancing of the structure. SEM–EDS data for both compounds are in agreement with single crystal structure refinements, although the calcium percentage is slightly elevated due to residual flux on the crystal surfaces. Calcium and tellurium within $Ca_6Te_3N_2$ have average ratios of 68% and 32%, respectively. For $Ca_6(Li_xFe_{1-x})Te_2N_3$, calcium and tellurium ratios are consistently 72% and 22% respectively. The iron content of $Ca_6(Li_xFe_{1-x})Te_2N_3$ ranges from 2.7% to 6.3% across multiple samples. The majority of values fall in the 4–6.3% range with occasional outliers at the lower atomic percentages when nickel contamination is present. Nickel incorporation from using steel crucibles ranges from 0.5% to 2.5%. Iron content of $Ca_6(Li_xFe_{1-x})Te_2N_3$ synthesized in niobium crucibles is consistent in the 5.5–6.3% range and shows no nickel contamination.

DOI: 10.1021/jacs.6b06024
J. Am. Chem. Soc. 2016, 138, 10636–10644

Crystallographic Analysis. Samples of $Ca_6Te_3N_2$ and $Ca_6(Li_xFe_{1-x})Te_2N_3$ were brought out of the glovebox under Parabar cryoprotectant oil (Hampton Research) and examined under a microscope to select crystals for diffraction studies. Pieces of suitable size were cut from larger crystals and were mounted in cryoloops. Single-crystal X-ray diffraction data were collected at 150 K under a stream of nitrogen using a Bruker APEX 2 CCD diffractometer with a Mo Kα radiation source. Absorption corrections were applied to the data sets using the SADABS program.[30] Refinements of the structures were performed using the SHELXTL package.[31] The structure of $Ca_6Te_3N_2$ was initially solved in monoclinic space group $C2/c$ (No.15), but use of the AddSym program in the PLATON software suite indicated the presence of additional symmetry elements and converted the structure to rhombohedral space group $R\bar{3}c$ (No. 167).[32] The structure of $Ca_6(Li_xFe_{1-x})Te_2N_3$ was solved in tetragonal space group $P4_2/m$ (No. 84). For both structures, calcium and tellurium sites were located using direct methods. Light element positions were located using difference Fourier calculations. Nitrogen atom sites were initially assigned as carbon, but higher than 100% occupancy was observed. Bond lengths and requirements of charge-balancing indicated the possibility that these were in fact nitrogen sites; this was confirmed after carbon-free syntheses were carried out which successfully yielded the target products. The Wyckoff site 2*b* in $Ca_6(Li_xFe_{1-x})Te_2N_3$ is located between two symmetry equivalent nitride sites and was originally thought to be a partially occupied calcium atom, but the bond lengths were too short. Upon finding iron present in the EDS analysis and noting similar Fe−N and Li−N bond lengths in the literature (vide infra), this site was assigned as occupied by a mixture of iron and lithium. Data sets were collected for several crystals, with the Fe content on this mixed site ranging from 52.5(4)% to 57.5(4)%, averaging 55% (for an average stoichiometry of $Ca_6Li_{0.45}Fe_{0.55}Te_2N_3$). Crystallographic data and collection parameters are shown in Table 1. Atomic positions and thermal parameters for both structures can be found in Supporting Information. Further details of the crystal structure investigations may be obtained from FIZ Karlsruhe, 76344 Eggenstein-Leopoldshafen, Germany (fax: (+49)7247-808-666; e-mail: crysdata@fiz-karlsruhe.de, on quoting the deposition number CSD-431001 (for $Ca_6Te_3N_2$) and CSD-431002 (for $Ca_6Li_{0.48}Fe_{0.52}Te_2N_3$).

Electronic Structure Calculations. Band structure and density of states (DOS) calculations for the title compounds were carried out using the Stuttgart TB-LMTO-ASA software package, based on the unit cell dimensions and atomic coordinates derived from single crystal diffraction data.[33] $Ca_6(Li_xFe_{1-x})Te_2N_3$ contains an iron/lithium mixed site (Wyckoff 2*b* site). Because the mixed occupancy is close to 50:50, an ordered model was developed in which iron and lithium alternate in this position. This was done by removing the symmetry to convert the Fe/Li 2*b* Wyckoff site into two crystallographically unique 1*a* sites, which were assigned as filled with Fe and Li. Calculations were carried out on the resulting $Ca_{12}LiFeTe_4N_6$ model in $P1$. For comparison, calculations on the two end member compounds were carried out in the original $P4_2/m$ symmetry: one model with the mixed site fully occupied with iron and the other model with lithium in this site ($Ca_6FeTe_2N_3$ and $Ca_6LiTe_2N_3$ respectively). Empty spheres were added by the program where appropriate to fill the unit cell volume. An 8 × 8 × 16 k-point mesh was used for the tetragonal structures and a 16 × 16 × 16 k-point mesh was used for the rhombohedral structure; these were integrated using the tetrahedron method. The basis sets for $Ca_6(Li_xFe_{1-x})Te_2N_3$ consisted of Ca 4s/4p/3d, Te 5s/5p/5d/4f, N 2s/2p/3s, and Fe 4s/4p/3d or Li 2s/2p/3s orbitals. The Ca 4p, Te 5d/4f, N 3s, and Li 2p/3s orbitals were downfolded. For $Ca_6Te_3N_2$, the basis sets consisted of Ca 4s/4p/3d, Te 5s/5p/5d/4f, and N 2s/2p/3s orbitals. The Ca 4p, Te 5d/4f, and N 3s were downfolded.

Magnetic Properties. Magnetic measurements were carried out on a Quantum Design SQUID magnetic property measurement system. Samples of $Ca_6(Li_{0.45}Fe_{0.55})Te_2N_3$ grown from Ca/Li/Te/C/Li_3N reactions in a 7:6:1:2:1 mmol ratio were taken out of the glovebox in Parabar oil, and large, clean crystals were selected under a microscope. The Parabar oil was wiped off of the crystals before sealing them between two pieces of kapton tape and placing this into a plastic straw attachment on the SQUID sample holder. Temperature dependent magnetic susceptibility data were collected between 1.8 and 200 K. A small signal at 50 K is due to sample holder impurity. A magnetic field of 5000 G was applied for the data collection. Field-dependent magnetization data were collected at 1.8 K between 0 and 7 T.

RESULTS AND DISCUSSION

Synthesis. Reactions of tellurium and a source of nitrogen in Ca/Li flux yielded two new complex metal nitrides: $Ca_6Te_3N_2$ and $Ca_6(Li_xFe_{1-x})Te_2N_3$. The $Ca_6Te_3N_2$ phase forms as glossy translucent chunks ranging in size from about 0.2 to 0.5 mm across. This material displays obvious dichroism, appearing green at some angles and red at others, depending on overhead angle of incident light when viewed under a microscope (see Figure 1c; both crystals were screened by SCXRD to confirm that they are in fact the same compound). The yield was 45% from Ca/Li/Te/Ca_3N_2 in a 3.5/3.5/0.5/0.5 mmol ratio based on tellurium; the byproduct was CaTe. The $Ca_6(Li_xFe_{1-x})Te_2N_3$ phase grows as black faceted rod crystals up to 0.6 mm in length and 0.2 mm in diameter. The yield is 50% (from Ca/Li/Te/C/Li_3N in a 7/6/1/2/1 ratio) based on nitrogen along with slight amounts of CaTe byproduct.

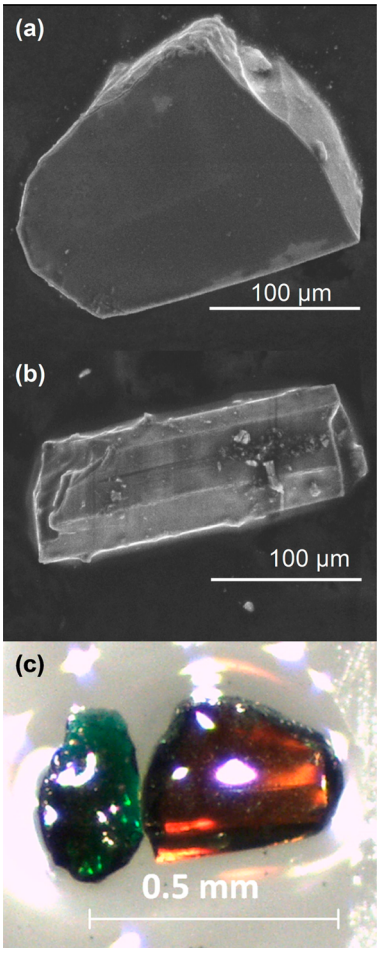

Figure 1. Images of $Ca_6Te_3N_2$ and $Ca_6(Li_xFe_{1-x})Te_2N_3$ crystals: (a) SEM image of $Ca_6Te_3N_2$; (b) SEM image of $Ca_6(Li_xFe_{1-x})Te_2N_3$; (c) Microscope image of $Ca_6Te_3N_2$ under parabar oil. Two colors, green and red, are observed due to inherent dichroism.

DOI: 10.1021/jacs.6b06024
J. Am. Chem. Soc. 2016, 138, 10636−10644

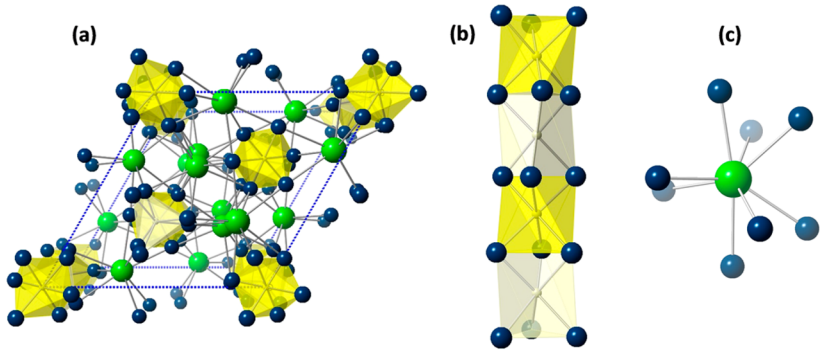

Figure 2. Structure of $Ca_6Te_3N_2$. (a) Rhombohedral structure of $Ca_6Te_3N_2$ viewed in the [001] direction. Calcium atoms are shown in blue, tellurium in green, and N@Ca_6 polyhedra in yellow. (b) Chain of alternating octahedral and trigonal prismatic N@Ca_6 polyhedra viewed in the [010] direction. (c) Eight-fold coordination environment of the Te site.

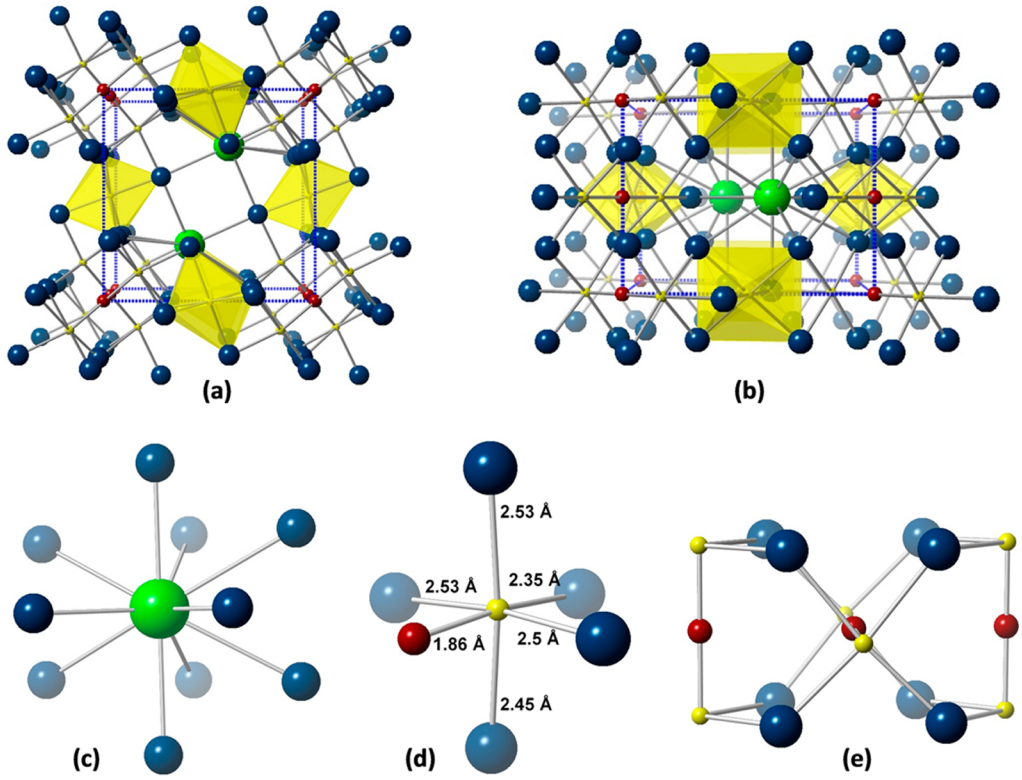

Figure 3. Structure of $Ca_6(Li_{0.48}Fe_{0.52})Te_2N_3$. Color scheme is the same as the rhombohedral structure with the exception of the addition of red spheres, which represent the Li^+/Fe^+ mixed site. Tetragonal structure viewed in (a) the [001] direction and (b) the [010] direction. (c) Tellurium anion coordination environment. (d) Local environment around N2, with bond lengths listed. (e) Linear N−(Fe/Li)−N units along the 4_2 screw axis.

Molten alkali or alkaline earth metals are clearly excellent reaction media for the synthesis of new nitrides. The successful isolation of nitrides from Ca/Li flux was anticipated by our previous accidental formation of $Ca_{14}As_6C_{0.45}N_{1.14}H_{4.91}$ during investigations into synthesis of arsenide carbides and hydrides.[25] Other examples of nitrides grown from melts of electropositive alkali and alkaline earth metals include Sr_2NiN_2, which crystallizes in molten Na, $Ca_3Ga_2N_4$, which was synthesized from a Ca/Na melt, $Li_2(Li_{1-x}Fe_x)N$, which was grown from excess molten Li, and subnitrides such as $Li_{80}Ba_{39}N_9$ and Na_5Ba_3N, which form in Li/Ba and Na/Ba flux, respectively.[28,34−37] Jesche and Canfield have explored both lithium and calcium melts for the synthesis of many binary and ternary nitrides.[38] The electropositive metals are effective at reducing N_2 or dissolving binary nitride reactants, coordinating the nitride anions, bringing them into solution and enabling the formation of complex metal nitride products. It was noted by Canfield that multinary nitride syntheses in pure calcium melts are hindered by formation of Ca_2N as a competing byproduct;[38] our use of Ca/Li flux mixtures appears to minimize the formation of this phase.

Structure of $Ca_6Te_3N_2$. $Ca_6Te_3N_2$ crystallizes in the rhombohedral space group $R\bar{3}c$ (shown in Figure 2). Its structure is an anti-type of the rinneite structure ($K_3NaFeCl_6$), as well as that of a family of 2H-hexagonal perovskite related oxides exemplified by Sr_3LiNbO_6.[39,40] The calcium cations of $Ca_6Te_3N_2$ are positioned in the anion sites of the parent structures. The telluride and nitride anions are both surrounded

DOI: 10.1021/jacs.6b06024
J. Am. Chem. Soc. 2016, 138, 10636−10644

by calcium cations and occupy the cation sites of the parent structures. There are two unique nitride anions (sites 6*b* and 6*a*, respectively), both coordinated by six calcium cations; N(1)@Ca_6 octahedra and N(2)@Ca_6 trigonal prisms share faces to form chains running in the [001] direction (Figure 2b). In the parent structures, these chains are comprised of octahedra centered by the smaller cation (for instance, $FeCl_6$ octahedra in rinneite and NbO_6 octahedra in Sr_3LiNbO_6) alternating with trigonal prisms centered by the larger cation ($NaCl_6$ and LiO_6 units, respectively). In $Ca_6Te_3N_2$, the Ca−N bond lengths are 2.3833(6)Å for the octahedrally coordinated nitrogen (N1) and 2.4990(6) Å for the trigonal prismatic coordination (N2). These Ca−N distances are within the range of bond lengths reported for $Ca_{14}As_6X_7$ (X = C, H, N) (2.265−2.608 Å), Ca_2N (2.4426 Å), $Ca_{11}N_6(CN_2)_2$ (2.308−2.9 Å), and Ca_3N_2 (2.4573−2.4792 Å).[25,41−43] The tellurium anion (18*e* site) is surrounded by eight calcium cations at bond lengths ranging from 3.2031(8) to 3.3374(9) Å to form an irregular polyhedron shown in Figure 2c. The tellurium site is positioned on the 3_2 screw axis running parallel to the *c*-axis. This screw axis is surrounded by chains of face-sharing N@Ca_6 polyhedra; the Te anions fill the spaces between these chains. The formation of $Ca_6Te_3N_2$ in a 2H-hexagonal perovskite anti-type is intriguing, given the inherent structural flexibility of this family of oxides. Variants of this structure are known with different ratios and stacking patterns of the octahedra and trigonal prisms.[40] Stacking variants may be accessible in the nitride systems by replacing tellurium with a smaller anion.

Structure of $Ca_6(Li_xFe_{1-x})Te_2N_3$. $Ca_6(Li_xFe_{1-x})Te_2N_3$ has a new structure type in tetragonal space group $P4_2/m$ (Figure 3). This compound also features telluride and nitride anions surrounded by calcium sites. The single unique tellurium site is coordinated to 10 calcium atoms with bond distances ranging from 3.251(1) to 3.652(1) Å. The N1 nitride site (2*d* Wyckoff site) is octahedrally coordinated to six Ca^{2+} cations at distances of 2.373(1)−2.4383(8) Å. An additional nitride site (4*j*) is octahedrally coordinated by five calcium atoms and a sixth site that was difficult to assign. Based on its position (linearly coordinated by two symmetry equivalent nitride anions at distances of 1.859(2) Å), this site (2*b*) must be occupied by a cationic species. The short bond length and low electron density indicates this site is occupied by a smaller and lighter cation than calcium. However, the electron density was higher than could be accounted for by lithium. Since SEM−EDS indicates the presence of iron, this was refined as a Li/Fe mixed site. Elemental analyses and crystallographic refinements on several crystals indicate a narrow substitution range on this site, from 52% to 57% Fe. A +1 oxidation state is required on this iron ion to balance the charge: $(Ca^{2+})_6(Li/Fe^{1+})_1(Te^{2-})_2(N^{3-})_3$.

This $Ca_6MTe_2N_3$ (M = Fe/Li) structure can be viewed as a stuffed anti-type of the Tl_3BiCl_6 structure (which is a simpler variant of the $(NH_4)_3MoCl_6$ structure type).[44] The calcium cations of $Ca_6(Li_xFe_{1-x})Te_2N_3$ occupy the chloride sites of Tl_3BiCl_6, and one of the nitride sites (on the 2*c* Wyckoff site) occupies the bismuth position. The tellurium anions are in the 4*j* Wyckoff site, in the same position as one of the thallium sites in Tl_3BiCl_6. The mixed site (M = Fe/Li) is positioned on the other thallium site of the parent structure (the cuboid-coordinated 2*b* Wyckoff site). These structural components yield a formula of $(Te_2M)NCa_6$, mirroring the stoichiometry of Tl_3BiCl_6. The remaining nitrogen site (on a 4*j* Wyckoff site), which linearly coordinates the Fe/Li cation, is not found in the parent structure; $Ca_6MTe_2N_3$ is therefore a "stuffed" variant.

Nitride compounds containing Fe^{1+} have been of great recent interest. This is largely due to the rarity of the monovalent iron ion and the unusual magnetism recently observed for this ion in $Li_2(Li_{1-x}Fe_x)N$, vide infra. This substitution compound of Li_3N was originally synthesized by Kniep et al; this group has gone on to isolate several other complex nitrido ferrates that also feature Li/Fe mixing, such as $Ca_2\{Li[(Li_{1-x}Fe_x)N_2]\}$ (x = 0.82), $Ca\{Li_2[(Li_{1-x}Fe_x)N]_2\}$ (x = 0.30), and $Sr\{Li_2[(Li_{1-x}Fe_x)N]_2\}$ (x = 0.46).[16,45,46] These compounds contain N−(Fe/Li)−N linear units linked into infinite chains, unlike the discrete N−(Li/Fe)−N species surrounded by calcium and organized along a screw axis in $Ca_6(Li_xFe_{1-x})Te_2N_3$. Other structures that feature isolated transition metal−nitride units include Li_4FeN_2, Sr_2FeN_2, Sr_2ZnN_2, and Ba_2ZnN_2.[47−49] Isolated linear units with Fe^{1+} are rarer with $Sr_6FeC_2N_7$ being the only other example.[50] The (Li/Fe)−N bond distance of 1.859(2) Å in $Ca_6(Li_{0.48}Fe_{0.52})Te_2N_3$ is very similar to Fe−N and Li−N distances of 1.8469(9)Å reported for $Ca_2\{Li[(Li_{1-x}Fe_x)N_2]\}$ with x = 0.82.[45] Li−N bond lengths at the 1*b* Wyckoff site in Li_3N are 1.938(1) Å but have been shown by Kniep et al. to decrease with increasing iron substitution at the Li site to 1.815(1) Å in $Li_2(Li_{0.37}Fe_{0.63})N$.[16,51]

Magnetic Properties of $Ca_6(Li_{0.45}Fe_{0.55})Te_2N_3$. Iron as Fe^{1+} exhibits abnormally high magnetic moments in some compounds, particularly when linearly coordinated by nitride anions. A linearly coordinated high spin d^7 ion is expected to have S = 3/2 and a spin-only magnetic moment of 3.87μ_B. Reports on Fe^+-substituted Li_3N analogs $Li_2(Li_{0.84}Fe_{0.16})N$ and $Li_2(Li_{0.79}Fe_{0.21})N$ indicated magnetic moments of 4.4μ_B/Fe and 5.8μ_B/Fe respectively, due to the presence of unquenched orbital angular momentum.[28,29] Depending on the level of iron substitution, some of these compounds exhibit large magnetic anisotropy and ferromagnetic ordering with coercive fields above 10 T, rivaling or exceeding the hard magnetic properties of rare-earth based magnets such as $Nd_2Fe_{14}B$.[28]

$Ca_6(Li_xFe_{1-x})Te_2N_3$ adds to the small number of compounds containing Fe^{1+} ions linearly coordinated by nitride anions. Magnetic susceptibility data for this compound are shown in Figures 4 and 5. Temperature dependence measurements show that $Ca_6(Li_{045}Fe_{0.55})Te_2N_3$ is paramagnetic with no long-range ordering down to 1.8 K and no difference between field-

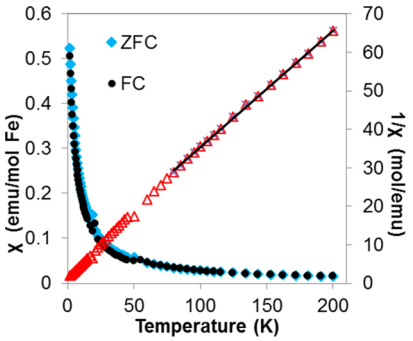

Figure 4. Temperature dependent magnetic susceptibility data for $Ca_6(Li_{0.45}Fe_{0.55})Te_2N_3$, collected at 0.5 T. Solid symbols are susceptibility data; empty red triangles are inverse susceptibility values, with the data fitted to the Curie−Weiss law indicated by the line.

DOI: 10.1021/jacs.6b06024
J. Am. Chem. Soc. 2016, 138, 10636−10644

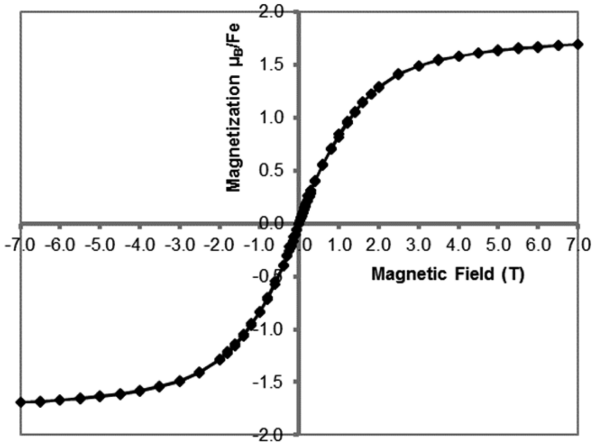

Figure 5. Magnetization data for $Ca_6(Li_{0.45}Fe_{0.55})Te_2N_3$, collected at 1.8 K.

cooled/zero-field cooled susceptibility. Fitting the high temperature data to the Curie–Weiss law yields a magnetic moment of $\mu_{eff} = 5.16\mu_B$/Fe ion and a Weiss constant of $\theta = -17$ K. The high magnetic moment on Fe^{1+} was reproducibly observed in measurements on several different samples; magnetic moments for the iron ranged from 4.29 to $5.16\mu_B$. This is in accordance with the reported magnetic moments on Fe^{1+} ions in substituted Li_3N. The somewhat large and negative Weiss constant may indicate that antiferromagnetic coupling forces are present between the Li/Fe sites, which are 3.36 Å apart. The lack of long-range ordering is likely due to the mixing of iron with lithium in the chain, which causes dilution of magnetic centers and may cause spin frustration.

The magnetization data for $Ca_6(Li_{0.45}Fe_{0.55})Te_2N_3$ at 1.8 K is shown in Figure 5. Despite the lack of evidence for long-range ordering in the temperature dependence data, magnetic saturation for $Ca_6(Li_{0.45}Fe_{0.55})Te_2N_3$ is clearly apparent at fields higher than 3T. The saturation magnetization is below $2\mu_B/Fe^{1+}$, which is contrary to the magnetic moment calculated from the Curie–Weiss fit above. This may be due to the highly anisotropic nature of the N–Fe–N linear units running down the *c*-axis and the inability to align this axis parallel to the applied magnetic field. Crystals proved cumbersome to align with the magnet due to their small sizes (multiple crystals were required to obtain measurements) and their air sensitivity, which hinders the ability to manipulate the orientation of the crystals. Crystals were inevitably oriented randomly, which inhibits complete magnetic saturation along an easy axis.

Further exploration of the transition metal substitution chemistry of $Ca_6(Li_{1-x}Fe_x)Te_2N_3$ is in progress. The syntheses described in this work were carried out in the presence of excess iron (using steel crucibles or with addition of excess iron reactant), which would likely maximize the iron content of the samples. Incorporation of smaller amounts is of interest; reports on $Li_2(Li_{1-x}Fe_x)N$ indicate that higher moments and hard ferromagnetic behavior is observed for analogs with lower iron content.[28] Li_3N is also able to substitute other transition metals (including Mn, Co, Ni, and Cu).[52,53] Our observation of nickel incorporation by EDS indicates the same is likely for $Ca_6(Li_{1-x}Fe_x)Te_2N_3$. It is also notable that the structure and magnetic properties of $Ca_6(Li_{1-x}Fe_x)Te_2N_3$ meet the design

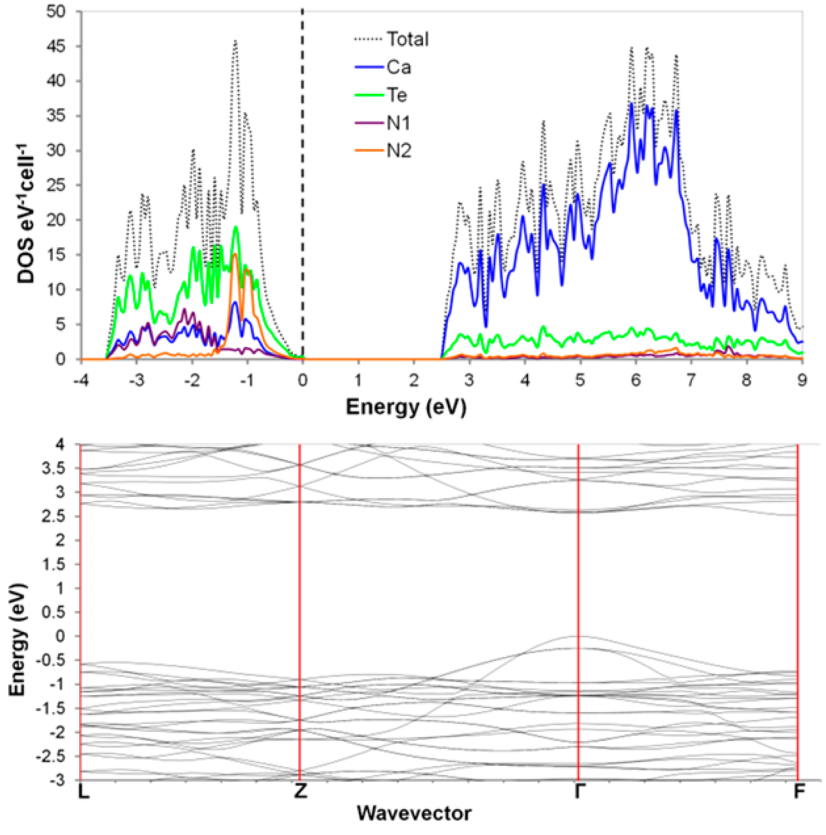

Figure 6. (top) Calculated electronic density of states data for $Ca_6Te_3N_2$. The Fermi level is set at 0 eV. (bottom) Calculated band structure of $Ca_6Te_3N_2$. Direct band gap is seen at Γ.

DOI: 10.1021/jacs.6b06024
J. Am. Chem. Soc. 2016, 138, 10636–10644

requirements for single chain magnets (SCM). These magnets are similar to single molecule magnets but acquire higher dimensionality (1D) due to the presence of a linker (such as a bidentate organic ligand) between each magnetic center, which orders the centers into chains. SCM behavior requires the presence of a magnetic ion with significant uniaxial anisotropy (the Ising center); these Ising centers must be linked in a way that produces nonzero interactions between the magnetic moments along the chain, and these chains must be separated in space to minimize any magnetic interactions between chains.[54] SCM behavior is typically targeted and explored in transition metal coordination polymer systems. While there is no covalent linker present in $Ca_6(Li_{1-x}Fe_x)Te_2N_3$, the positioning of the strongly anisotropic N−Fe−N units along the 4_2 screw axis in the crystal structure creates a 1-D chain of these magnetic species, and the chains are separated in space by the calcium/tellurium network.

Electronic Structure and Optical Properties. In agreement with the charge-balanced nature of $Ca_6Te_3N_2$ ($(Ca^{2+})_6(Te^{2-})_3(N^{3-})_2$), band structure and density of states data shown in Figure 6 confirm that this compound is a semiconductor with a calculated band gap of E_g = 2.5 eV. Calcium states dominate the conduction band but have minor contributions to the valence band near the Fermi level (E_F). The anions in the structure make the major contributions to the valence band. Tellurium states are predominant between 0 and −0.5 eV below E_F. Bands derived from the trigonal prismatically coordinated N2 ion are found between −0.5 and −1.5 eV; the octahedrally coordinated N1 site yields bands at lower energies (−1.5 to −3.5 eV). This can be explained by the relative Ca−N bond lengths; the octahedral site has shorter Ca−N bond lengths than the trigonal prismatic site. The improved orbital overlap causes stabilization of the N1 states.

The band structure indicates that $Ca_6Te_3N_2$ is a direct gap semiconductor. This direct gap occurs at the Γ point, from valence band tellurium states to calcium states in the conduction band. The strongly anisotropic nature of the compound is indicated by the fact that, while the tellurium states at the Γ point yield a band gap of 2.5 eV, the effective bandgap in all other directions in the Brillouin zone is significantly larger. Accordingly, $Ca_6Te_3N_2$ displays dichroism, appearing red at some angles of incident light and green at others (Figure 1). Polarized UV/vis/NIR measurements on aligned samples would be needed to further investigate this but are hindered by the air sensitivity of this compound. Such measurements have been carried out on other compounds exhibiting dichroism, including chalcopyrites such as $AgGaSe_2$ and $CdGeP_2$, and more recently on layered black phosphorus.[55−57] These compounds exhibit band structures that are strongly anisotropic near E_F, and strong changes in absorbance edge are observed with different light polarizations.

Calculation and analysis of the electronic structure of $Ca_6(Li_xFe_{1-x})Te_2N_3$ was more difficult due to the mixed Li/Fe site. Since the ratio of lithium to iron in this 2*b* Wyckoff site is very close to 1:1, an ordered model was developed by lowering the symmetry. This converts the 2*b* site to two individual 1*a* sites, one of which was assigned as lithium and the other as iron. This produces a structure with alternating [N−Fe−N] and [N−Li−N] units along the *c*-axis. The resulting density of states data are shown in Figure 7. Similar to $Ca_6Te_3N_2$, the valence bands near E_F are dominated by tellurium states, and the conduction bands by calcium states. However, there is no bandgap; instead, there is a narrow band

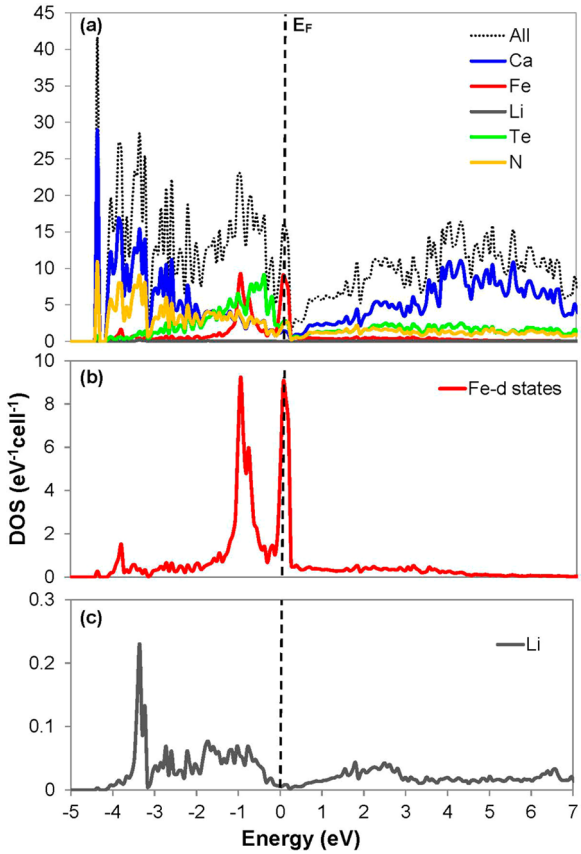

Figure 7. Electronic density of states data calculated for $Ca_6(Li_{0.5}Fe_{0.5})Te_2N_3$ model compound with ordered Li and Fe siting. The Fermi level is set at 0 eV. (a) Total and partial DOS. (b) The iron d-orbital derived states. (c) The lithium states.

at the Fermi level derived from iron d_{z^2} orbitals. Another narrow d-orbital band is found at 1 eV below E_F. As expected from the structure, not all of the d-orbitals show interactions with states from the neighboring nitride ions. The d_{xy}, $d_{x^2-y^2}$, d_{xz}, and d_{yz} orbitals contributing to the −1 eV band are essentially nonbonding, but the d_{z^2} orbital (at or slightly above E_F) does hybridize with nitride states. Based on these calculations, the black color of the crystals is due to the iron substitution, but the narrow band and dilution with lithium localizes the d-electrons on iron sites, in agreement with the magnetic susceptibility data.

In addition to density of states calculations for the ordered $Ca_6Li_{0.5}Fe_{0.5}Te_2N_3$ model, calculations were also done for models in which the 2*b* site of the $P4_2/m$ structure was either fully occupied by Li or fully occupied by Fe. The resulting DOS plots are shown in the Supporting Information as Figure S2. The model with the Li/Fe site fully occupied by lithium ($Ca_6LiTe_2N_3$) shows salt-like characteristics and a band gap of 1.8 eV, as expected for a charge-balanced compound consisting of only main group elements. The valence band is comprised predominantly of anion states (N^{3-}, Te^{2-}) and the conduction band contains the cationic states (Ca^{2+} and Li^+). The model containing iron filling the mixed site ($Ca_6FeTe_2N_3$) shows large contributions of iron d-orbital valence states in a narrow band crossing the Fermi level.

DOI: 10.1021/jacs.6b06024
J. Am. Chem. Soc. 2016, 138, 10636−10644

CONCLUSIONS

Two complex metal nitrides with new structure types were grown from calcium/lithium melts. The syntheses of $Ca_6Te_3N_2$ and $Ca_6(Li_xFe_{1-x})Te_2N_3$, along with our previously reported nitride $Ca_{14}As_6C_{0.45}N_{1.14}H_{4.91}$, demonstrate the capability of Ca/Li flux to dissolve nitride salts and enable the crystallization of new metal nitride materials. $Ca_6Te_3N_2$ features a direct band gap of 2.5 eV according to DOS calculations, making it a potential candidate for semiconductor applications such as LEDs. $Ca_6(Li_xFe_{1-x})Te_2N_3$ features a large magnetic moment on a linearly coordinated iron ion in the rare +1 oxidation state. Unfortunately, further measurements such as UV−vis measurements for $Ca_6Te_3N_2$ and magnetic measurements of oriented crystals of $Ca_6(Li_xFe_{1-x})Te_2N_3$ were limited by their air-sensitive nature. Synthetic routes to analogs of $Ca_6(Li_xFe_{1-x})Te_2N_3$ containing different amounts of iron at the Li/Fe site may be interesting, possibly enabling variation of the magnetic moment of Fe^{1+} and yielding long-range magnetic ordering, as is observed for $Li_2(Li_{1-x}Fe_x)N$.[28]

ASSOCIATED CONTENT

Supporting Information

The Supporting Information is available free of charge on the ACS Publications website at DOI: 10.1021/jacs.6b06024.

Tables of atomic positions and displacement factors, powder diffraction data, density of states data for $Ca_6MTe_2N_3$ (M = Fe or Li) (PDF)

Additional crystallographic data for the title phases (CIF)

AUTHOR INFORMATION

Corresponding Author

*latturner@chem.fsu.edu

Notes

The authors declare no competing financial interest.

ACKNOWLEDGMENTS

This research was supported by the NSF Division of Materials Research (Grant Number DMR-14-10214). This work made use of the scanning electron microscope facilities of the Biological Sciences Imaging Resource in the FSU Biology Department; we thank Dr. Eric Lochner for his assistance with this equipment.

REFERENCES

(1) Gorczyca, I.; Suski, T.; Christensen, N. E.; Svane, A. *Appl. Phys. Lett.* **2010**, *96*, 101907.

(2) Bryden, W. A.; Kistenmacher, T. J.; Wickenden, D. K.; Morgan, J. S.; Wickenden, A. E.; Ecelberger, S. A.; Poehler, T. O. *Johns Hopkins APL Technol. Dig.* **1989**, *10* (1), 3−13.

(3) Maruska, H. P.; Rhines, W. C. *Solid-State Electron.* **2015**, *111*, 32−41.

(4) Matthias, B. T.; Hulm, J. K. *Phys. Rev.* **1952**, *87* (5), 799−806.

(5) Ziegler, W. T.; Young, R. A. *Phys. Rev.* **1953**, *90* (1), 115−119.

(6) Frazer, B. C. *Phys. Rev.* **1958**, *112* (3), 751−754.

(7) Kim, T. K.; Takahashi, M. *Appl. Phys. Lett.* **1972**, *20* (12), 492.

(8) Abe, H.; Cheung, T.; Bell, A. T. *Catal. Lett.* **1993**, *21* (1−2), 11−18.

(9) Wang, S.; Ge, H.; Sun, S.; Zhang, J.; Liu, F.; Wen, X.; Yu, X.; Wang, L.; Zhang, Y.; Xu, H.; Neuefeind, J. C.; Qin, Z.; Chen, C.; Jin, C.; Li, Y.; He, D.; Zhao, Y. *J. Am. Chem. Soc.* **2015**, *137* (14), 4815−4822.

(10) Tabata, M.; Maeda, K.; Higashi, M.; Lu, D.; Takata, T.; Abe, R.; Domen, K. *Langmuir* **2010**, *26* (12), 9161−9165.

(11) Soignard, E.; McMillan, P. F.; Chaplin, T. D.; Farag, S. M.; Bull, C. L.; Somayazulu, M. S.; Leinenweber, K. *Phys. Rev. B: Condens. Matter Mater. Phys.* **2003**, *68* (13), 132101.

(12) Bull, C. L.; McMillan, P. F.; Soignard, E.; Leinenweber, K. *J. Solid State Chem.* **2004**, *177* (4−5), 1488−1492.

(13) Friedrich, A.; Winkler, B.; Bayarjargal, L.; Morgenroth, W.; Juarez-Arellano, E. A.; Milman, V.; Refson, K.; Kunz, M.; Chen, K. *Phys. Rev. Lett.* **2010**, *105* (8), 085504.

(14) Miura, A.; Lowe, M.; Leonard, B. M.; Subban, C. V.; Masubuchi, Y.; Kikkawa, S.; Dronskowski, R.; Hennig, R.; Abruna, H.; Disalvo, F. J. *J. Solid State Chem.* **2011**, *184*, 7−11.

(15) Barsoum, M. W. *Prog. Solid State Chem.* **2000**, *28* (1−4), 201−281.

(16) Klatyk, J.; Kniep, R. *Z. Kristallogr. - New Cryst. Struct.* **1999**, *214* (4), 447−448.

(17) DiSalvo, F. J.; Clarke, S. J. *Curr. Opin. Solid State Mater. Sci.* **1996**, *1* (2), 241−249.

(18) Gregory, D. H. *J. Chem. Soc., Dalton Trans.* **1999**, *3*, 259−270.

(19) Barker, M. G.; Grazia Francesconi, M.; O'Meara, P. M.; Baker, C. F. *J. Alloys Compd.* **2001**, *317−318*, 186−189.

(20) Musil, J.; Baroch, P.; Vlček, J.; Nam, K. H.; Han, J. G. *Thin Solid Films* **2005**, *475* (1−2), 208−218.

(21) Kanatzidis, M. G.; Pöttgen, R.; Jeitschko, W. *Angew. Chem., Int. Ed.* **2005**, *44*, 6996−7023.

(22) Blankenship, T. V.; Dickman, M. J.; van de Burgt, L. J.; Latturner, S. E. *Inorg. Chem.* **2015**, *54* (3), 914−921.

(23) Blankenship, T. V.; Chen, B.; Latturner, S. E. *Chem. Mater.* **2014**, *26* (10), 3202−3208.

(24) Blankenship, T. V.; Lita, A.; Latturner, S. E. *Inorg. Chem.* **2012**, *51* (24), 13345−13350.

(25) Blankenship, T. V.; Wang, X.; Hoffmann, C.; Latturner, S. E. *Inorg. Chem.* **2014**, *53* (19), 10620−10626.

(26) Lang, D. A.; Latturner, S. E. *Eur. J. Inorg. Chem.* **2011**, *2011* (26), 4006−4011.

(27) Lang, D. A.; Zaikina, J. V.; Lovingood, D. D.; Gedris, T. E.; Latturner, S. E. *J. Am. Chem. Soc.* **2010**, *132* (49), 17523−17530.

(28) Jesche, A.; McCallum, R. W.; Thimmaiah, S.; Jacobs, J. L.; Taufour, V.; Kreyssig, A.; Houk, R. S.; Bud'ko, S. L.; Canfield, P. C. *Nat. Commun.* **2014**, *5*, 3333.

(29) Klatyk, J.; Schnelle, W.; Wagner, F. R.; Niewa, R.; Novák, P.; Kniep, R.; Waldeck, M.; Ksenofontov, V.; Gütlich, P. *Phys. Rev. Lett.* **2002**, *88* (20), 207202.

(30) *SAINT*, version 6.02a; Bruker AXS Inc.: Madison WI, 2000.

(31) Sheldrick, G. M. *SHELXTL NT/2000*, version 6.1; Bruker AXS, Inc.: Madison WI, 2000.

(32) Spek, A. L. *Acta Crystallogr., Sect. D: Biol. Crystallogr.* **2009**, *D65*, 148−155.

(33) (a) Jepsen, O.; Burkhardt, A.; Andersen, O. K. Program *TB-LMTO-ASA*, version 4.7; Max-Planck-Institut für Festkörperforschung: Stuttgart, Germany, 2000. (b) Blöchl, P. E.; Jepsen, O.; Andersen, O. K. *Phys. Rev. B: Condens. Matter Mater. Phys.* **1994**, *49*, 16223−16233.

(34) Kowach, G. R.; Brese, N. E.; Bolle, U. M.; Warren, C. J.; DiSalvo, F. J. *J. Solid State Chem.* **2000**, *154*, 542−550.

(35) Clarke, S. J.; DiSalvo, F. J. *Inorg. Chem.* **1997**, *36*, 1143−1148.

(36) Smetana, V.; Babizhetskyy, V.; Vajenine, G.; Simon, A. *Inorg. Chem.* **2006**, *45* (26), 10786−10789.

(37) Snyder, G. J.; Simon, A. *J. Am. Chem. Soc.* **1995**, *117*, 1996−1999.

(38) Jesche, A.; Canfield, P. C. *Philos. Mag.* **2014**, *94* (21), 2372−2403.

(39) Beattie, J. K.; Moore, C. J. *Inorg. Chem.* **1982**, *21*, 1292−1295.

(40) Zur Loye, H. C.; Zhao, Q.; Bugaris, D. E.; Chance, W. M. *CrystEngComm* **2012**, *14*, 23−39.

(41) Gregory, D. H.; Bowman, A.; Baker, C. F.; Weston, D. P. *J. Mater. Chem.* **2000**, *10* (7), 1635−1641.

(42) Reckeweg, O.; DiSalvo, F. J. *Angew. Chem., Int. Ed.* **2000**, *39* (2), 412−414.

(43) Laurent, Y.; Lang, J.; Lebihan, M. T. *Acta Crystallogr., Sect. B: Struct. Crystallogr. Cryst. Chem.* **1968**, *24* (4), 494−499.

DOI: 10.1021/jacs.6b06024
J. Am. Chem. Soc. 2016, 138, 10636−10644

(44) Beck, J.; Benz, S. *Z. Anorg. Allg. Chem.* **2010**, *636*, 928−935.
(45) Klatyk, J.; Kniep, R. *Z. Kristallogr. - New Cryst. Struct.* **1999**, *214* (4), 451−452.
(46) Klatyk, J.; Kniep, R. *Z. Kristallogr. - New Cryst. Struct.* **1999**, *214* (4), 449−450.
(47) Gudat, A.; Kniep, R.; Rabenau, A. *Angew. Chem., Int. Ed. Engl.* **1991**, *30* (2), 199−200.
(48) Höhn, P.; Kniep, R. *Z. Naturforsch., B: J. Chem. Sci.* **1992**, *47* (4), 477−481.
(49) Yamane, H.; DiSalvo, F. J. *J. Solid State Chem.* **1995**, *119* (2), 375−379.
(50) Bendyna, J. K.; Höhn, P.; Kniep, R. *Z. Kristallogr. - New Cryst. Struct.* **2009**, *224* (1), 5−6.
(51) Rabenau, A.; Schulz, H. *J. Less-Common Met.* **1976**, *50* (1), 155−159.
(52) Klatyk, J.; Kniep, R. *Z. Kristallogr. - New Cryst. Struct.* **1999**, *214* (4), 445−446.
(53) Jesche, A.; Ke, L.; Jacobs, J. L.; Harmon, B.; Houk, R. S.; Canfield, P. C. *Phys. Rev. B: Condens. Matter Mater. Phys.* **2015**, *91*, 180403.
(54) Dhers, S.; Feltham, H. L. C.; Brooker, S. *Coord. Chem. Rev.* **2015**, *296*, 24−44.
(55) Choi, I.-H.; Han, S.-D.; Eom, S.-H.; Lee, W.-H. *J. Korean Phys. Soc.* **1996**, *29* (3), 377−383.
(56) Shay, J. L.; Buehler, E.; Wernick, J. H. *Phys. Rev. B* **1971**, *4* (8), 2479−2485.
(57) Qiao, J.; Kong, X.; Hu, Z.-X.; Yang, F.; Ji, W. *Nat. Commun.* **2014**, *5*, 4475.

DOI: 10.1021/jacs.6b06024
J. Am. Chem. Soc. 2016, 138, 10636−10644